UC Berkeley

UC Berkeley Previously Published Works

Title

TaO x electron transport layers for CO 2 reduction Si photocathodes

Permalink

https://escholarship.org/uc/item/7hf8m2k7

Journal

Journal of Materials Chemistry A, 11(25)

ISSN

2050-7488

Authors

Prabhakar, Rajiv Ramanujam
Lemerle, Raphaël
Barecka, Magda
et al.

Publication Date

2023-06-27

DOI

10.1039/d3ta01028g

Copyright Information

This work is made available under the terms of a Creative Commons Attribution-ShareAlike License, available at https://creativecommons.org/licenses/by-sa/4.0/

Peer reviewed

eScholarship.org Powered by the California Digital Library
University of California

# $TaO_x$ electron transport layers for $CO_2$ reduction Si photocathodes

*Rajiv Ramanujam Prabhakar,[a,b,#] Raphaël Lemerle,[a,b,c,#] Magda Barecka,[d,e,f] Minki Kim,[a,b,g] Sehun Seo[a,b], Elif Nur Dayi,[a,b,c] Irene Dei Tos,[a,b] and Joel W. Ager,[a,b,h,i,*]*

[a]Liquid Sunlight Alliance, Lawrence Berkeley National Laboratory, Berkeley, California 94720, United States

[b]Chemical Sciences Division, Lawrence Berkeley National Laboratory, Berkeley, California 94720, United States

[c]Materials Science and Engineering, École Polytechnique Fédéral de Lausanne, Lausanne 1015, Switzerland

[d]Department of Chemical Engineering, Northeastern University, 360 Huntington Avenue, 02215 Boston, USA; email: m.barecka@northeastern.edu

[e]Department of Chemistry and Chemical Biology, Northeastern University, 360 Huntington Avenue, 02215 Boston, USA

[f]Cambridge Centre for Advanced Research and Education in Singapore, CARES Ltd., 1 CREATE Way, CREATE Tower #05-05, 138602, Singapore.

[g]Chemical and Biomolecular Engineering, Korea Advanced Institute of Science and Technology (KAIST), Daejeon 34141, Republic of Korea

[h]Department of Materials Science and Engineering, University of California, Berkeley, Berkeley, CA 94720, USA

[i]Materials Sciences Division, Lawrence Berkeley National Laboratory, Berkeley, California 94720, United States

AUTHOR INFORMATION

# These authors contributed equally

**Corresponding Author**

*jwager@lbl.gov (J. W. Ager)

KEYWORDS: Photoelectrochemistry, $CO_2$ reduction, charge selective contacts, $TaO_x$

## ABSTRACT

Electron transport layers (ETLs) used as components of photocathodes for light-driven $CO_2$ reduction ($CO_2R$) in aqueous media should have good electronic transport, be stable under $CO_2R$ conditions, and, ideally, be catalytically inert for the competing hydrogen evolution reaction (HER). Here, using planar p-Si (100) as the absorbing material, we show that $TaO_x$ satisfies all three of the above criteria. $TaO_x$ films were synthesized by both pulsed laser deposition (PLD) and radio-frequency (RF) sputtering. In both cases, careful control of the oxygen partial pressure during growth was required to produce ETLs with acceptable electron conductivity. p-Si/$TaO_x$ photocathodes were interfaced with ca. 10 nm of a $CO_2R$ catalyst: Cu or Au. Under front illumination with simulated AM 1.5G in $CO_2$-saturated bicarbonate buffer, we observed, for both metals, faradaic efficiencies for $CO_2R$ products of ~50% and ~30% for PLD $TaO_x$ and RF sputtered $TaO_x$, respectively, at photocurrent densities up to 8 mA $cm^{-2}$. p-Si/$TiO_2$/Cu photocathodes were also evaluated but produced mostly $H_2$ (>97%) due to reduction of the $TiO_2$ to Ti metal under $CO_2R$ conditions. In contrast, a dual ETL photocathode (p-Si/$TiO_2$/$TaO_x$/Cu) was selective for $CO_2R$, which suggests a strategy for separately optimizing selective charge collection and the stability of the ETL/water interface. The maximum photovoltage obtained with p-Si/$TaO_x$/Cu devices was 300 mV which was increased to 430-460 mV by employing ion implantation to make $pn^+$-Si$TaO_x$/Cu structures. Photocathodes with RF sputtered $TaO_x$ ETLs are stable for $CO_2R$ for at least 300 min. Techno-economic analysis shows that the reported system, if scaled, could allow for an economically viable production of feedstocks for chemical synthesis under the adoption of specific $CO_2$ credit schemes, thus becoming a significant component to carbon-neutral manufacturing.

## INTRODUCTION

Charge selective contacts (CSC) provide the asymmetric necessary for light to electrical power conversion in photovoltaic (PV) solar cells.[1] For this reason, in silicon PV there is significant research focus and progress on engineering CSCs that provide both efficient charge collection and interface passivation.[2–5] Energy conversion with photoelectrochemical (PEC) devices operates on the same principle: the surfaces of photocathodes must be selective for electrons and the surface of photoanodes must be selective for holes. While some materials, notably metal oxides used as photoanodes for the oxygen evolution reaction (OER), provide charge selectivity via their intrinsic catalytic activity for the desired reaction, engineered surface layers are also widely employed.[6,7]

For PEC electrodes, in addition to charge carrier selectivity, there are two additional constraints for CSCs. Firstly, the CSC must be stable in the electrochemical environment (often either strong base or acid) so that it can serve as a "protection" layer for the photoabsorber if it is a kinetically or thermodynamically unstable material during operation.[8] Further, the CSC either by itself or in combination with a co-catalyst must provide selectivity to the desired reaction, for instance hydrogen evolution reaction (HER), oxygen evolution reaction (OER) or $CO_2$ reduction ($CO_2R$). Additionally, for the case of PEC $CO_2R$, since both HER and $CO_2R$ are thermodynamically possible, the CSC or, more specifically, the electron transport layer (ETL) in combination with a co-catalyst must be selective to $CO_2R$ products rather than HER.

There are numerous experimental reports which utilize a Si/ETL/co-catalyst stack to form photocathodes for HER.[9–11] $TiO_2$ and either Pt or Ru are typical choices for the ETL and HER catalyst, respectively. To make a photocathode which will instead reduce $CO_2$, the co-catalyst should be replaced with a metal which is more active for $CO_2R$ than for HER.[12,13] For instance, Au has been reported to drive $CO_2R$ more selectively towards CO,[14] Bi towards formate,[15,16] and Cu towards C-C coupled products like $C_2H_4$.[13,17] However, there are comparatively fewer reports on

the functioning of these catalysts when integrated with $CO_2R$ photocathodes. Hinogami et al.[18] interfaced p-Si with Cu, Ag, and Au without any ETL and found faradaic efficiencies (FEs) of up to ca. 30% for formate and methane for Cu and up to 50% for CO for Ag. Qiu et al.[19] reported a p-InP/$TiO_2$/Cu photocathode which, intriguingly, produced methanol at ca. 5% FE. Gurudayal et al.[20] reported a Si photocathode with a $TiO_2$ ETL and Cu-Ag bimetallic catalyst which produced up to 80% selectivity for $C_2$+ products. However, in this case, the thick catalyst layer was optically opaque so that illumination from the back (dry) side was employed.

It thus remains an unmet challenge to make a selective $CO_2R$ photocathode capable of front (wet) side illumination. Having an optically thin co-catalyst layer would minimize the photoelectrode cost and allowing for the photocathode to be illuminated from the front side (wet side).[21] This would be particularly advantageous when employing low-cost light absorbers with short minority carrier diffusion lengths. In our initial attempts to make such a device we used p-Si/$TiO_2$ interfaced with Cu and Ag. However, under operation, the $TiO_2$ was reduced to Ti metal, which then dominates the catalytic activity and produces $H_2$ (FE > 97%).

We then examined the Si PV literature to find an oxide ETL which would be more stable than $TiO_2$; $TaO_x$ appeared promising. When interfaced to Si, it has a small conduction band offset (desirable for electron collection) and large valence band offset (desirable for hole blocking) and is reported to passivate surface states.[22–24] Si PV cells incorporating an n-Si/$TaO_x$ heterocontact have been reported to have up to 19% power conversion efficiency.[22] $TaO_x$ has also been used as an ETL for photocathodes. Wang et al[25] reported that a $pn^+$ -Si/$Ta_2O_5$/Pt photocathode was stable for over 200 hours while generating $H_2$. Riyajuddin et al[26] reported 10 hours of stability under HER conditions for a Si nanowire/$Ta_2O_5$/N-doped graphene quantum dot photocathode.

The prior PV and PEC HER work with $TaO_x$ suggests that it may be a good candidate for an ETL for PEC $CO_2R$ devices. Moreover, examination of its Pourbaix diagram under typical $CO_2$

reduction ($CO_2R$) conditions (-1 V vs. SHE and pH 7) predicts that it will be stable.[27,28] There is also considerable synthesis flexibility. $TaO_x$ thin films have been prepared by a variety of techniques like pulsed laser deposition (PLD)[29], RF sputtering[30] and atomic layer deposition (ALD)[31] and its electronic conductivity can be tuned (from insulating to semiconducting) by controlling the concentration of oxygen vacancies.[32]

These considerations motivated us to study p-Si/$TaO_x$ photocathodes interfaced with thin (optically transparent) metal $CO_2R$ catalysts (p-Si/$TaO_x$/Cu). We synthesized $TaO_x$ thin films using pulsed laser deposition (PLD) and reactive radio frequency (RF) sputtering techniques. Stoichiometric $Ta_2O_5$ films had poor electronic transport which was improved by controlling the oxygen partial pressure during deposition. Under simulated AM 1.5G illumination, the $TaO_x$ ETL-based Si photocathodes (synthesized by both PLD and RF sputtering) had good selectivity to $CO_2R$ products, ~50% and ~30% respectively, which we attribute to the stability and inertness of the $TaO_x$. Using ion implanted contacts onto silicon photocathodes with $TaO_x$ ETLs higher photovoltages were obtained (p-Si/$n^+$/$TaO_x$/Cu ~ 430 mV and $p^+$/n-Si/$n^+$/$TaO_x$/Cu ~ 460 mV) when compared to p-Si/$TaO_x$ junction (~ 300 mV). We found that the photocathodes were quite sensitive to contamination from metal crossover from the anode due to the small catalyst loading needed for optical transparency and that this could be mitigated by using a non-noble metal counter electrode (graphite). We identify stability as a key challenge for this type of solar to chemical energy conversion approach and provide scale-up scenarios informed by a technoeconomic analysis.

## RESULTS AND DISCUSSION

**$TiO_2$ as an ETL for $CO_2R$ Si photocathodes with a thin Cu catalyst.** In initial work, we investigated the $CO_2R$ product distribution of a p-Si photocathode with an atomic layer deposition (ALD) $TiO_2$ as an ETL and a thin 10 nm Cu co-catalyst. PEC measurements were performed in 0.1

M $KHCO_3$ electrolyte under 1 sun illumination for Si photocathodes (these conditions were used throughout the study, see Detailed Methods section in the SI). Such a photocathode shows a photocurrent onset at ~ -0.05 V vs RHE and a photocurrent density of ~ 12 mA $cm^{-2}$ at -1 V vs RHE (**Figure 1a).** However, the expected products from $CO_2R$ on Cu are not observed. Instead, the major product is $H_2$ (FE >97%, **Figure 1b**).

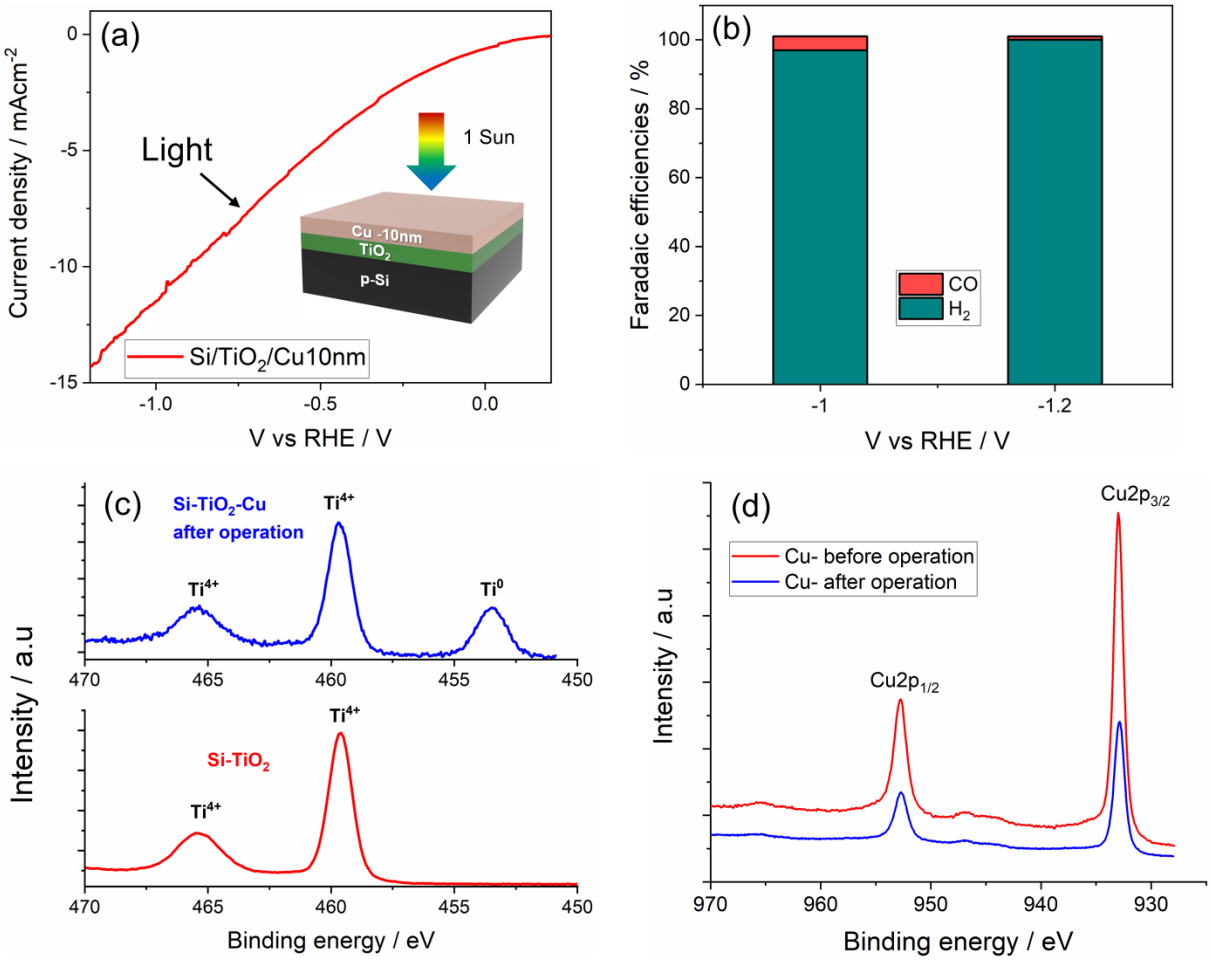


**Figure 1.** (a) Current density ($J$) vs Voltage ($V$) plots for Si/$TiO_2$/Cu10 nm under 1 sun illumination in 0.1 M $KHCO_3$ (b) Faradaic efficiencies of $CO_2R$ products for pSi/$TiO_2$/Cu10 nm (c) Ti 2p core level spectra of Si-$TiO_2$ (as prepared from ALD) and Si-$TiO_2$-Cu10nm after $CO_2R$ photo electrolysis for 230 mins under 1 sun illumination in 0.1M $KHCO_3$ at -1.0 V vs RHE (d) Cu 2p

core level spectra of Si-$TiO_2$-Cu10nm before and after operation under 1 sun illumination in 0.1 M $KHCO_3$ at -1.0 V vs RHE.

We hypothesized that the $H_2$ formation was due to the activity of Ti metal, which is known to be active for HER.[13] Indeed, we see experimental evidence that when $TiO_2$ is in contact with the electrolyte (0.1 M $KHCO_3$) under $CO_2R$ conditions, it is reduced to Ti metal as evidenced by the prominent $Ti^0$ peak in the Ti 2p core level spectra after operation (**Figure 1c**). Before $CO_2R$ operation the $TiO_2$ was completely covered by the Cu catalyst as evidenced by the absence of Ti XPS peaks (**Figure S2**). However, during $CO_2R$ operation, the $TiO_2$ layer was gradually exposed to the electrolyte as evidenced by the observation of Ti XPS peaks after operation (**Figure 1c**). Evidently, the HER activity on the Ti outcompetes $CO_2R$ on the Cu, which remain unmodified after operation (**Figure 1d**).

We investigated the effect of increasing the thickness of the Cu layer, understanding that this will eventually limit the photocurrent density in the front illumination geometry which we employed. Upon increasing the Cu thickness to 15 nm (**Figure S3 (a)**), we observed a marginal improvement with $CO_2R$ FEs of ca. 10%. Further increases in the metal thickness would be expected to greatly reduce the photocurrent (**Figure S3 (b)**). We concluded that $TiO_2$ is not a suitable ETL for $CO_2R$ photocathodes operated under the conditions we have employed and thus explored $TaO_x$ as an alternative.

**Pulsed Laser Deposition (PLD) grown $TaO_x$ as an ETL for p-Si $CO_2R$ photocathodes:** Next, we synthesized $TaO_x$ films on p-Si by PLD using a stoichiometric $Ta_2O_5$ target (details in SI). Substoichiometric $Ta_2O_5$ has been reported to exhibit higher electronic conductivity than more stoichiometric material due to the presence of oxygen vacancies.[33] Therefore, different $O_2$ flow rates were employed in the PLD chamber as shown schematically in **Figure 2 (a)**. We denote $TaO_x$ grown by PLD on p-Si with 0.1 sccm, 0.3 sccm and 1.6 sccm oxygen flow as $TaO_x$-0.1, $TaO_x$-0.3

and $TaO_x$-1.6. As expected from prior reports on PLD-grown $TaO_x$ without any annealing step,[34] XRD patterns (**Figure S4)** were featureless, indicating that the films are amorphous.

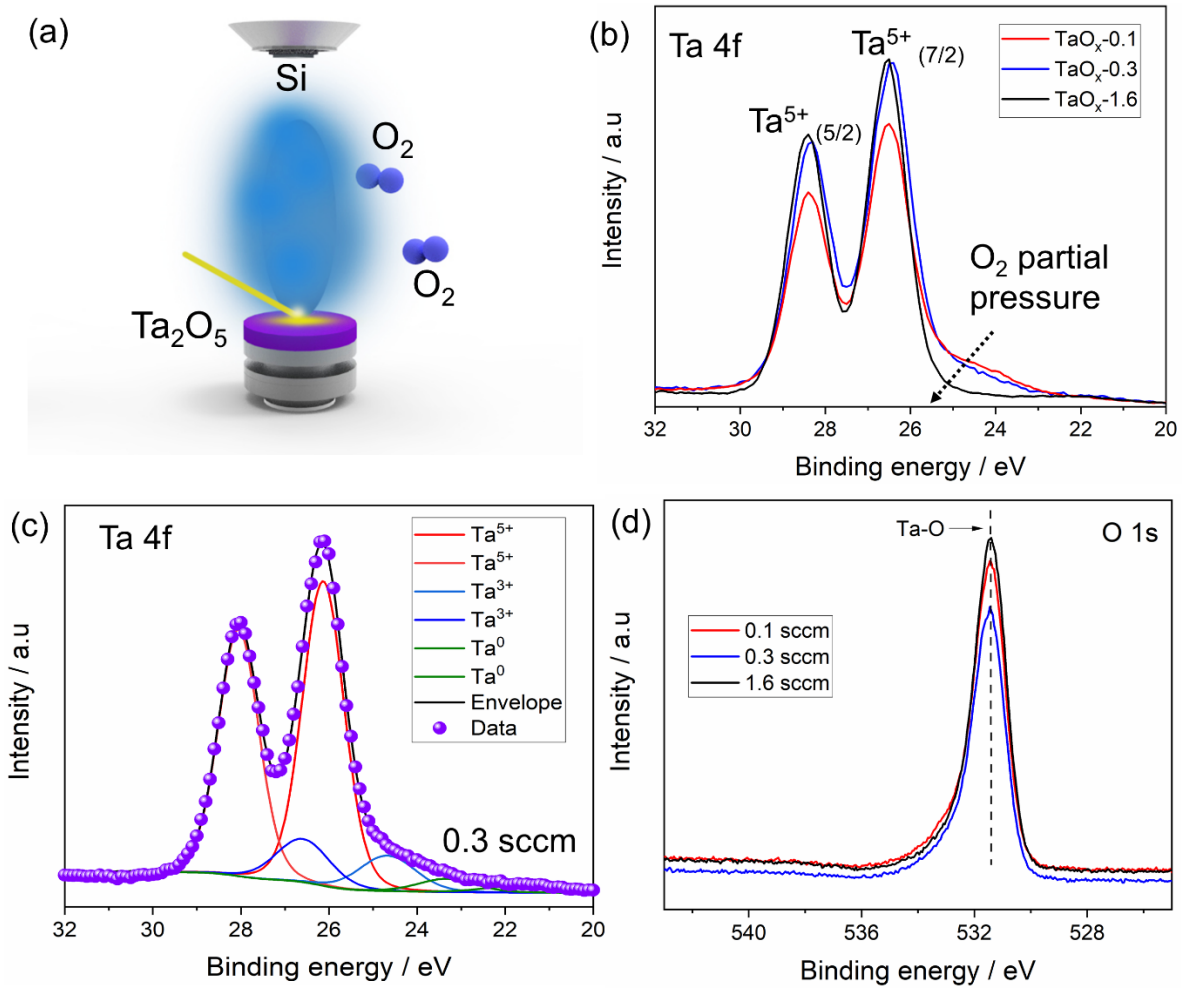


**Figure 2.** (a) Schematic of PLD deposition of $TaO_x$ (b) XPS core level spectra of Ta 4f for PLD-grown $TaO_x$ grown at different oxygen flow rates (c) XPS core level spectra of Ta 4f for $TaO_x$-0.3(d) XPS core level spectra of O1s for PLD-grown $TaO_x$ at different oxygen flow rates.

Chemical composition was evaluated with X-ray photoelectron spectroscopy (XPS). We assign the doublet peak observed at 28.3/26.4 eV for all films (**Figure 2 (b)**) to Ta 4f 7/2 and Ta 4f 5/2 from the $Ta^{5+}$ oxidation state.[35] A notable feature of the Ta 4f spectra is the presence of a shoulder peak at between 25 eV and 23 eV which decreases with increasing $O_2$ flow rate in the PLD

chamber. We assign this feature to sub-oxides of Ta which are expected to be formed in substoichiometric $Ta_2O_5$ films.[36]

Higher flow rates of $O_2$ (1.6 sccm) yielded a more stoichiometric $Ta_2O_5$ film as evidenced by the absence of suboxides of tantalum oxide. **Figure 2 (c)** shows the deconvolution of the Ta 4f spectra of $TaO_x$-0.3. Focusing on the shoulder at lower binding energy, the peaks at 26.4 eV and 24.5 eV are attributed to the $Ta^{3+}$ oxidation state.[30,37] The O 1s spectrum was fitted with two gaussian components with peaks at 530.9 eV and 532 eV which would correspond to Ta-O binding and surface contaminations/ peroxide $O_2^{2-}$ (**Figure S5**).[22,35] No obvious difference was observed for the O 1s spectra for the different $O_2$ flow rates of the $TaO_x$ films (**Figure 2 (d)**) with the peak position of the Ta-O binding remaining the same for all thin films. Our XPS results shows that the stoichiometry of $TaO_x$ could be controlled by varying the $O_2$ flow rate in the PLD chamber.

Next, we fabricated p-Si photocathodes with the PLD-grown $TaO_x$ as the ETL and Cu co-catalyst. We chose a Cu catalyst thickness of 10 nm due to higher $CO_2R$ product yield and higher photocurrent density (despite having lower transmission of light to the photocathode than a 5 nm thick Cu co-catalyst) (**Figure S6-S8**). Si photocathodes with a $TaO_x$-0.3 ETL exhibited the highest photocurrent density under $CO_2R$ conditions reaching a maximum photocurrent density of ~ 7 mA $cm^{-2}$ (**Figure 3 (a)**). The photocurrent density of $TaO_x$-1.6 was lower than the $TaO_x$-0.3 due to its higher resistivity as result of a higher oxygen partial pressure during the PLD growth.[32,37]. This was verified by performing ultraviolet photoelectron spectroscopy (UPS) measurements to obtain the valence band spectra of $TaO_x$ (**Figure 3 (b)**). It is evident that the defect band in the band gap of $TaO_x$ increases with reduced oxygen partial pressure confirming the increase of oxygen vacancies for PLD $TaO_x$ grown with a 0.3 sccm $O_2$ flow rate. The p-Si/$TaO_x$/Cu-10nm based photocathode produced nearly 52 % $CO_2R$ products at bias of -1.2 V vs RHE while a p-Si/$TiO_2$

photocathode with the same Cu co-catalyst thickness yielded only $H_2$ (**Figure 4 (a)**) despite its earlier photocurrent onset and higher photocurrent density (**Figure S9**).

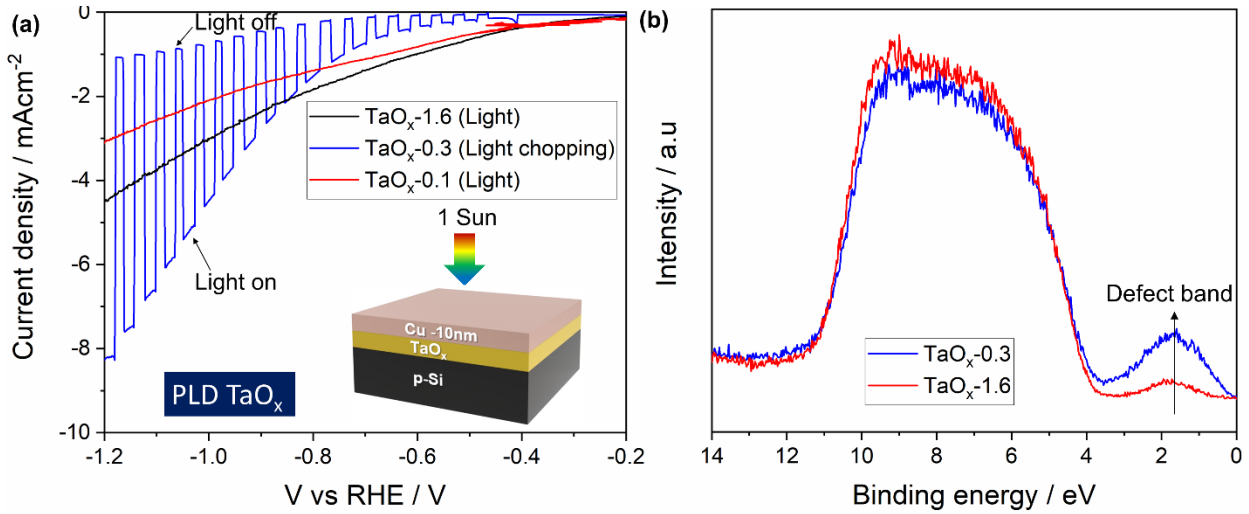


**Figure 3.** (a) Current density vs Voltage plots for p-Si/$TaO_x$/Cu 10nm photocathodes with $TaO_x$ grown ETLs at different oxygen flow rates under 1 sun illumination in a 0.1 M $KHCO_3$ electrolyte. (b) Valence band spectra of $TaO_x$-0.3 and $TaO_x$-1.6 thin films.

To evaluate the compatibility of $TaO_x$ with other $CO_2R$ catalysts, an Au catalyst was employed to evaluate the $CO_2R$ product distribution. A Ta underlayer was used for the Au catalyst to improve its adhesion to $TaO_x$. The photocurrent density obtained was similar to that of p-Si/$TaO_x$/Cu (**Figure S10**) and the $CO_2R$ products obtained were primarily C1products (CO, $HCOO^-$) as expected for an Au catalyst (**Figure 4 (b)**). Based on these results, $TaO_x$ could be employed as an ETL for p-Si interfaced with both Cu and Au co-catalysts for $CO_2R$.

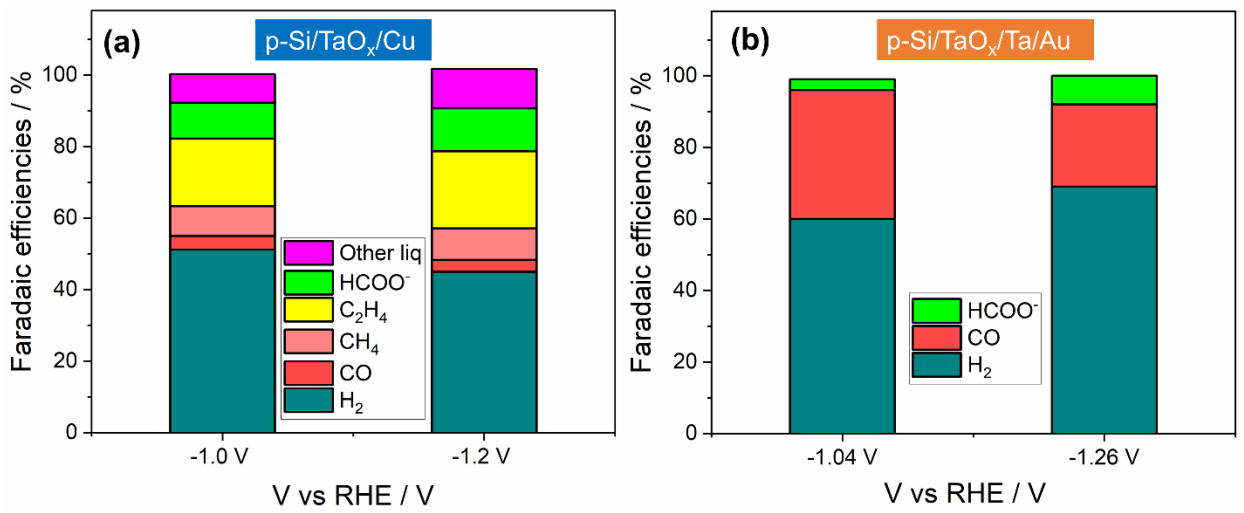


**Figure 4**. Faradaic efficiencies for (a) p-Si/$TaO_x$/Cu (other liq denotes ethanol and acetate) (b) p-Si/$TaO_x$/Ta/Au photocathodes under 1 sun illumination in 0.1 M $KHCO_3$

**Reactive radio frequency (RF) sputtered $TaO_x$ as an ETL for $CO_2$R Si photocathode.** Photocathodes were made with $TaO_x$ deposited by reactive RF sputtering, which is a more scalable technique than PLD (**experimental details in supporting information**). A Ta metal target was used and the Ar:$O_2$ ratio in the chamber was used to oxygen substoichiometry of $TaO_x$. **Figure 5 (a)** shows the Ta 4f spectra for the $TaO_x$ films prepared with 2 different Ar:$O_2$ ratios. Similar to the PLD prepared $TaO_x$ films (compare **Figure 2 (b)**), the doublet peaks for $Ta^{5+}$ oxidation state are dominant. However, the film made with a lower $O_2$ partial pressure (99:1 Ar:$O_2$) exhibits a significant peak corresponding to Ta metal suggesting that not all the Ta metal has been oxidized to the +5 oxidation state.

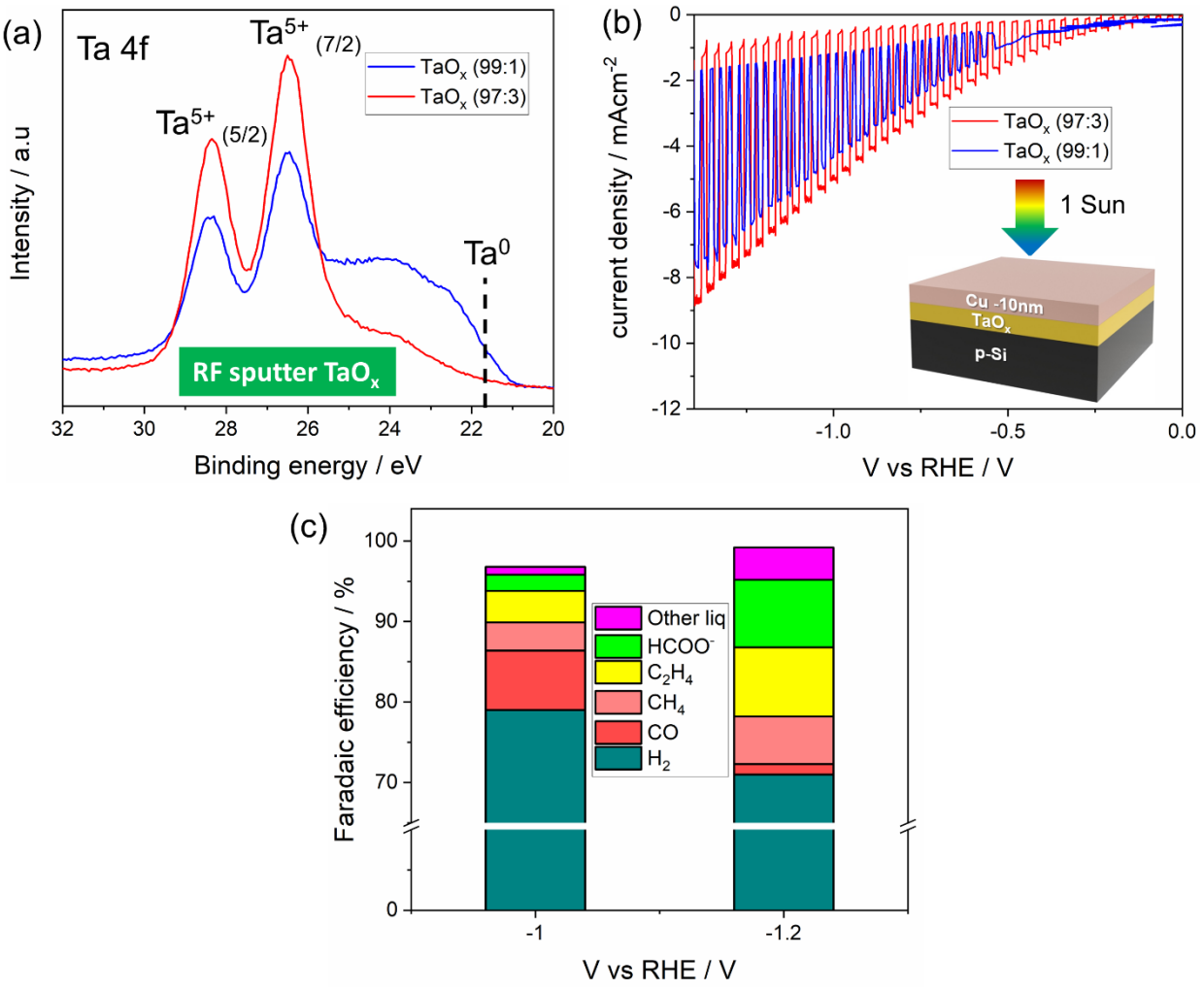


**Figure 5**. (a) Ta 4f core level spectra of $TaO_x$ prepared by RF sputtering under 2 different Ar: $O_2$ ratio (b) Current density (*J*) vs Voltage (*V*) plots for Si/$TaO_x$(20 nm)/Cu 10 nm under 1 sun illumination in 0.1 M $KHCO_3$ under 2 different Ar:$O_2$ concentration (c) Faradaic efficiencies of $CO_2R$ products for Si/$TaO_x$ (20 nm)/Cu10 nm under -1 V and -1.2 V vs RHE (other liq denotes ethanol and acetate).

Next the photoelectrochemical performance of the p-Si/$TaO_x$ (RFsputtered)/Cu photocathodes were evaluated under the same $CO_2R$ conditions as p-Si/$TaO_x$ (PLD grown)/Cu photocathodes. Photocathodes fabricated using RF sputtered TaOx had a very smooth surface after deposition of the Cu catalyst (**Figure S11**) and their XRD patterns only exhibited peaks corresponding to Si (**Figure S12**). The photocathode with higher oxygen content ($TaO_x$ 97:3) yielded a marginal higher

photocurrent and lower dark current as there is no Ta metal in the film when compared to $TaO_x$ (99:1) (**Figure 5 (b)**). Variation of the $TaO_x$ thickness showed that photocathodes with 20 nm $TaO_x$ yielded better fill factors and photocurrent density despite exhibiting similar substoichiometry **(Figure S13 and S14**). If the $TaO_x$ thickness is too thick as in the case of 40nm then the photocurrent density is lowered probably due to increased series resistance and if the thickness is below 20 nm then the coverage of $TaO_x$ on Si is not uniform. Hence a thickness of 20 nm of $TaO_x$ with 97:3 Ar to $O_2$ condition was found to be optimum. Upon comparing the champion device of sputtering ($TaO_x$ (97:3)) with PLD champion device ($TaO_x$-0.3), the sputtering champion device exhibited an earlier photocurrent onset but a marginally lower photocurrent density (**Figure S15**). This could be attributed to an increase in the substoichiometry of $TaO_x$ films prepared by sputtering (**Figure S16**).

**Si photocathode with dual ETL**: A dual ETL approach has shown promise in water splitting where one ETL serves as a n-type junction layer and the other performs the role of protection and catalyst support.[38] Since $TiO_2$ has a better band alignment with p-Si, we used it as the primary ETL and sputtered $TaO_x$ on it to take advantage of its higher $CO_2R$ product yield and stability. The photocurrent onset and the photocurrent density of such a dual ETL photocathode is lower in comparison to Si-$TiO_2$/Cu layer **(Figure 6 (a))**. But the dual ETL photocathode produced more $CO_2R$ products than a Si-$TiO_2$-Cu as the $TiO_2$ is buried under $TaO_x$. Since the $TiO_2$ layer is not fully exposed to the electrolyte under $CO_2R$ conditions, HER activity is suppressed and the catalytic activity could be dominated by the $TaO_x$/Cu layer **(Figure 6b)**. The dual ETL device was able to combine the earlier photocurrent onset of p-Si/$TiO_2$/Cu device with the higher $CO_2R$ product selectivity of p-Si/$TaO_x$/Cu device. The partial current densities towards $CO_2R$ products (CO, $CH_4$, $C_2H_4$ and $HCOO^-$) for dual ETL photocathode were only marginally lower than the p-Si-$TaO_x$-Cu photocathode at -1.0 V vs RHE (**Figure S17**). Having a dual ETL approach would

enable photocathode designs where the photovoltage could be improved by employing n-type layer which has a good band alignment with the underlying p-type absorber and simultaneously taking advantage of $TaO_x$/Cu's stability and higher yield of $CO_2R$ products.

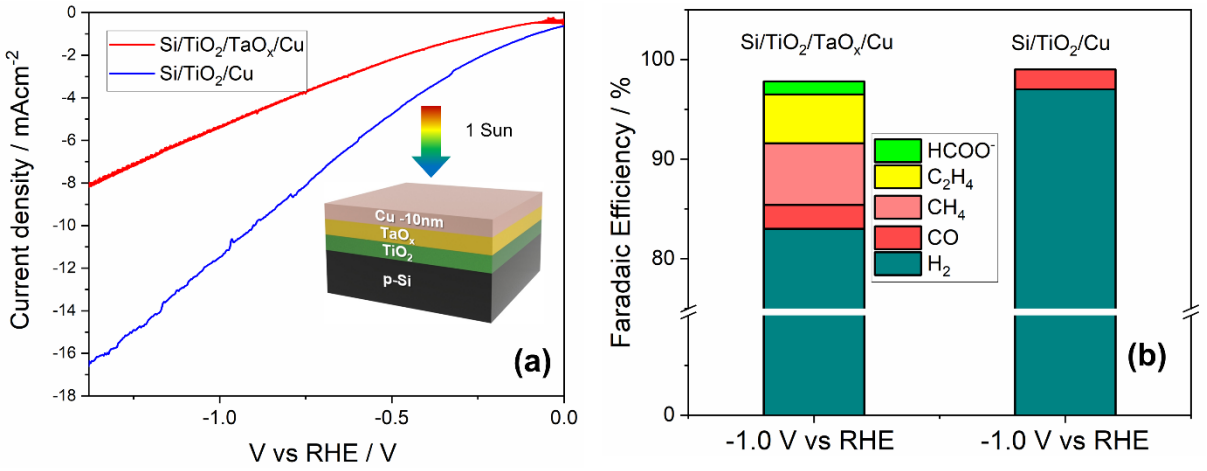


**Figure 6.** (a) Current density (*J*) vs Voltage (*V*) plots for Si/$TiO_2$/Cu and Si/$TiO_2$/$TaO_x$ (97:3)/Cu under 1 sun illumination in 0.1 M $KHCO_3$ (b) Faradaic efficiencies of $CO_2R$ products for Si/$TiO_2$/Cu and Si/$TiO_2$/$TaO_x$(97:3)/Cu The thickness of Cu catalyst used was 10 nm for both photocathodes.

**Photovoltage**: Finally, we fabricated a $n^+$Si/$TaO_x$ (97:3)/Cu dark cathode (black curve in Figure 7) so that we can compare the onset of the dark catalytic current to photocurrent onset of a p-Si/$TaO_x$/Cu photocathode (Figure 7 (a)). There are no reports in literature to the best of our knowledge where p-Si is directly interfaced with $TaO_x$ to form the p-n junction which gives a photovoltage. Instead, most reports in the photovoltaic literature employ n-Si with $TaO_x$ as a surface passivation/electron selective contact.[22] In this work a photovoltage of ~ 300 mV was obtained for p-Si/$TaO_x$ junctions with a Cu $CO_2R$ catalyst (**Figure 7 (a) and Figure S18 (a)**). To improve the photovoltage of these photocathodes, an $n^+$ implant of p-Si wafers was performed to yield a better-quality junction with RF sputtered $TaO_x$ onto the p-Si/$n^+$ with a Cu catalyst. This

photocathode yielded a higher photovoltage of 430 mV (**Figure 7 (b) and Figure S18 (b)**). Both photovoltage and photocurrent density was increased when a silicon photocathode (n-Si with $n^+$ and $p^+$ implanted contacts[20]) were employed with a RF-sputtered $TaO_x$ ETL and Cu catalyst (**Figure 7 (c) and Figure S18 (c)**) showing the broad applicability of RF-sputtered $TaO_x$ as an ETL for photocathodes.

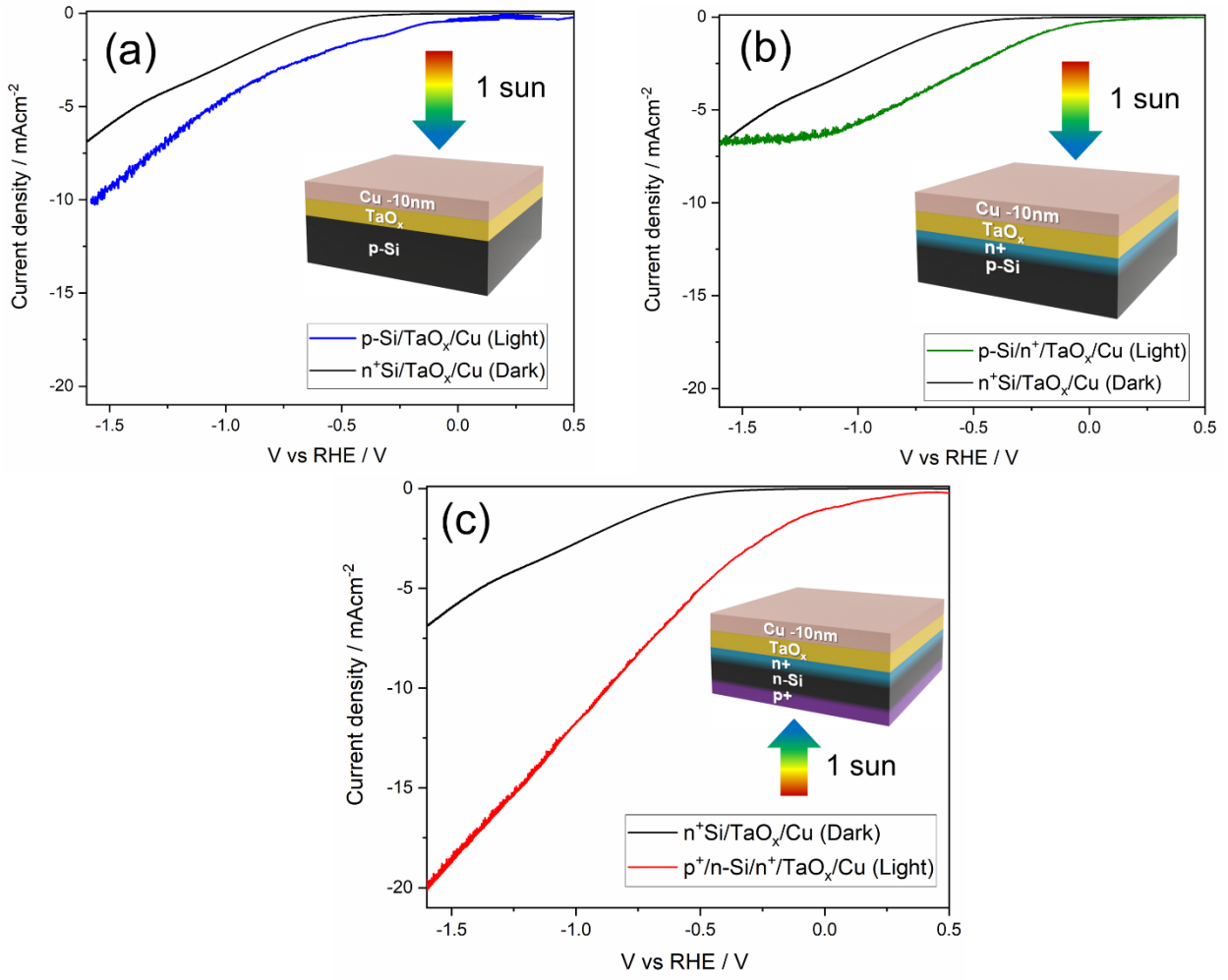


**Figure 7.** Current density vs voltage plots for (a) $n^+Si/TaO_x/Cu$ (dark cathode) and $p\text{-}Si/TaO_x/Cu$ (photocurrent), (b) $n^+Si/TaO_x/Cu$ (dark cathode) and $p\text{-}Si/n^+/TaO_x/Cu$ (photocathode) and (c) $n^+Si/TaO_x/Cu$ (dark cathode) and $p^+/n\text{-}Si/n^+/TaO_x/Cu$ (photocathode).

**Long-term stability of p-Si/$TaO_x$/Cu photocathodes:** The long-term stability of p-Si/$TaO_x$/Cu photocathodes over a period of 300 mins was evaluated by the time evolution of $CO_2R$ gaseous products (**Figure S19**). Samples with RF sputtered $TaO_x$ were chosen as it is more scalable synthesis technique than PLD and has a higher potential for commercialization. The surface of the photocathode became more rougher after the long term $CO_2R$ electrolysis (**Figure S20**). A fairly stable evolution of $CO_2R$ products was observed for at least for a period of 120 mins after which the faradaic efficiencies for the $CO_2R$ products decreased. The electrolyte was changed after 225 mins when no ethylene production was observed. Although there was a decrease in the Cu signal from XPS after operation (**Figure S21**), the lack of ethylene production could not be just attributed to loss of Cu catalyst. After $CO_2R$ photoelectrolysis, contact angle measurements were performed to investigate the hydrophobicity of the photocathode and it was observed that the surface of the photocathode ($TaO_x$/Cu) became more hydrophilic after $CO_2R$ (**Figure S22)**). In the $CO_2R$ electrolysis literature, the change in hydrophobicity has been attributed to minor $CO_2R$ product polymerization (acrolein to polyacrylic acid) on the surface of the Cu catalyst.[39] It is conceivable that this effect is occurring here, as well. In stability tests, we used a Pt counter electrode but found that Pt migration to the PEC surface strongly affected the results which are mitigated by using a graphite counter electrode (see discussion in SI).

Using a graphite counter electrode resulted in continued ethylene production even after 300 mins of operations (and good photocurrent stability **Figure S23**) when compared to Pt counter electrode which required change of electrolyte after 225 mins in order to sustain ethylene production (**Figure 8 (a)**). Further no Pt 4f peak (71 eV) was observed on the photocathode surface after 5 hours of operation when employing a graphite counter electrode (**Figure S24**). The surface of p-Si/TaOx/Cu after operation were still hydrophilic (same as the case with Pt counter electrode) hinting that the long-term stability of the photocathode was not significantly affected by the change

in hydrophobicity of the surface but rather the crossover of Pt from the counter electrode was the main reason for decreased $C_2H_4$ production (**Figure 8 (b) and (c)**).

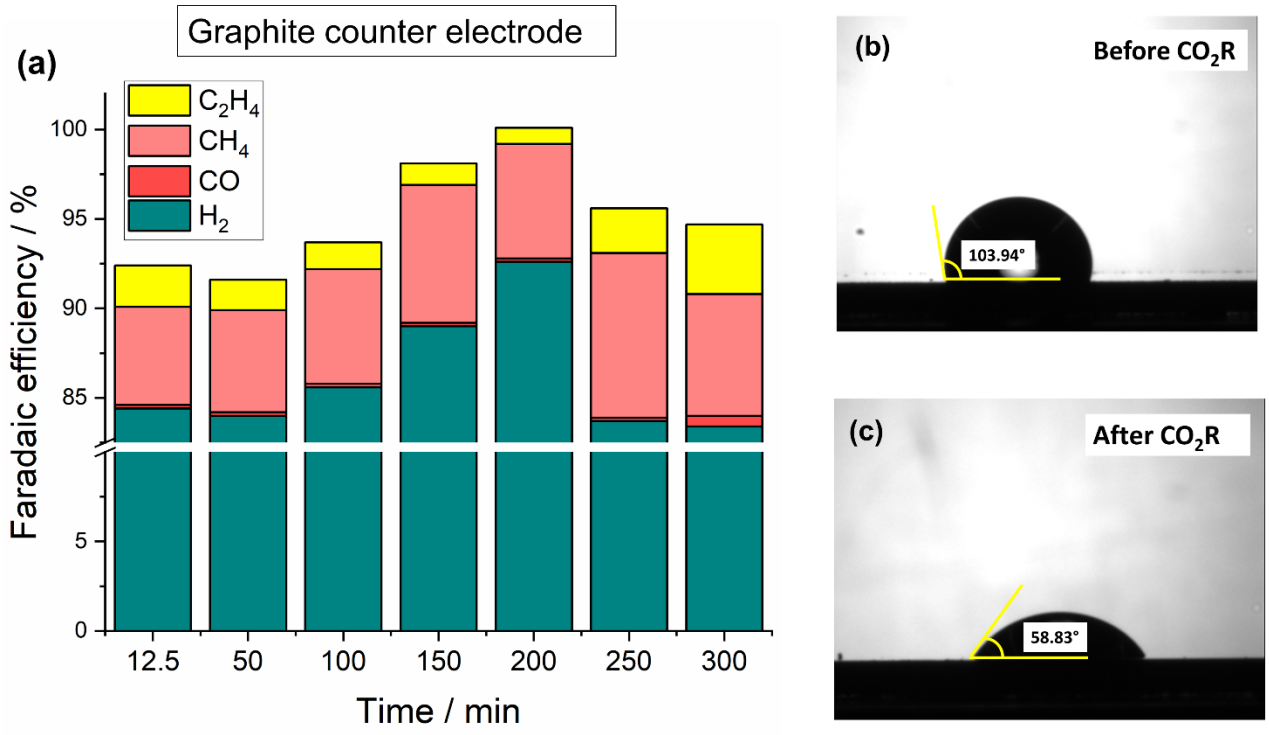


**Figure 8. (a)** Gaseous $CO_2R$ product distribution as a function of time for Si/$TaO_x$(97:3)/Cu10nm photocathode under 1 sun illumination in 0.1M $KHCO_3$ at -1.2 V vs RHE with a graphite counter electrode where the production of $C_2H_4$ remained steady after 300 mins of operation without any need of electrolyte change. Contact angle measurements of p-Si/$TaO_x$/Cu photocathode with a Pt counter electrode during $CO_2R$ measurements for (b) before $CO_2R$ and (c) after $CO_2R$ operation for 300 mins.

**Techno-economic analysis of Si-$TaO_x$-Cu photocathode:** The selectivity of Si-$TaO_x$-Cu photocathode towards carbon-containing products incentivized to conceptually design a large-scale photocatalytic system that could be used for production of carbon-rich gas streams from abundant, biogenic $CO_2$ (**Figure. 9(a)**). One of the anticipated bottlenecks towards the deployment of $CO_2$-

based systems is the low concentration of $CO_2$ in the ambient air.[40] The availability of $CO_2$ in oceans is significantly higher.[41] We thus conceptualized a system where ocean water, source of preconcentrated $CO_2$, circulates through photoelectrochemical systems, and $CO_2$ is converted into a stream of ethylene, carbon monoxide, methane, and hydrogen, being a useful input to various chemical manufacturing processes.[42] Such a system would require a minimum input of renewable electricity sourced from solar panels or windmills, as a significant amount of energy is being supplied via direct sunlight irradiation.

Looking towards this large-scale scenario, we sought to understand whether proposed catalyst deposition method could be effectively scaled up, and we assessed the cost of production of a system incorporating a thin $TaO_x$-Cu layer deposited on silicon wafer, using pilot plant scale/ semi-industrial coefficients for energy and gases use during physical vapor deposition process[43,44], and most recent price indicators for each component of the electrocatalytic system.[45–48] While other deposition methods reported here, such as RF sputtering, could further reduce the catalyst production cost, selecting physical vapor deposition (PVD) as reference allows to assess a less favorable scenario thus reduce the risk of overestimating the potential of the photocathode, being current at an early development stage. Given the excellent reduction of the thickness of the catalyst, the manufacturing cost becomes practically reduced to the cost of the silicon wafer and the membrane (**Figure 9(b)**), contributing together to >95% of the cost of the photoelectrode system (detail cost contributions in SI). Intriguingly, similar results have been obtained for Au-based electrodes (SI), showing that thin catalyst layers allow to drastically minimize the cost of metals used in catalyst development.

Looking at the return on investment into the proposed photoelectrochemical system, we deployed a recent protocol for the assessment of emerging electrolysis technologies (method details in SI) [49]. Our assessment is based on a model of a Si-$TaO_x$-Cu electrolyzer where 75% of supplied

$CO_2$ is being converted to a carbon-rich product, under experimentally reported 0.01 A $cm^{-2}$ of current density and applying an external voltage of 1.2 V. We assumed an average market price for this ethylene-rich stream, current renewable electricity price[42] between 0.02 – 0.05 $/kWh, and a broad range of $CO_2$ credit being paid for the avoided emissions of $CO_2$ (our system allows to avoid emissions of petroleum-based $CO_2$ by producing chemicals from biogenic $CO_2$). The sensitivity analysis **(Figure 9(c))** demonstrates that in presence of $CO_2$ credit schemes, return on investment is even less than 2 years, what provides an incentive for further research and optimization of $CO_2$ utilization methods. The decrease of the price of renewable electricity alone would not be sufficient to support these innovative approaches (see the grey area in **Figure 9 (c)**), depicting non-viable scenarios), and the availability of $CO_2$ credit will be critical for the growth of photoelectrochemical methods. Still, we need as well to address several scale-up challenges: demonstrate the capability to achieve increased $CO_2$ conversion level and avoid the formation of liquid products which will be more difficult to separate than the gaseous stream that we focus on. Importantly, electrolysis of sea water with a high concentration of salts might also lead to formation of chlorine on the anode. However, the studies focusing on the production of hydrogen from sea water demonstrated that it is possible to effectively block chlorine formation by the addition of $MnO_x$ into the anode structure.[50] Achieving the outstanding techno-economic metrics for the PEC system described here will thus necessitate coordinated efforts in further development of more scalable cathodes, anodes and related chemical process design.

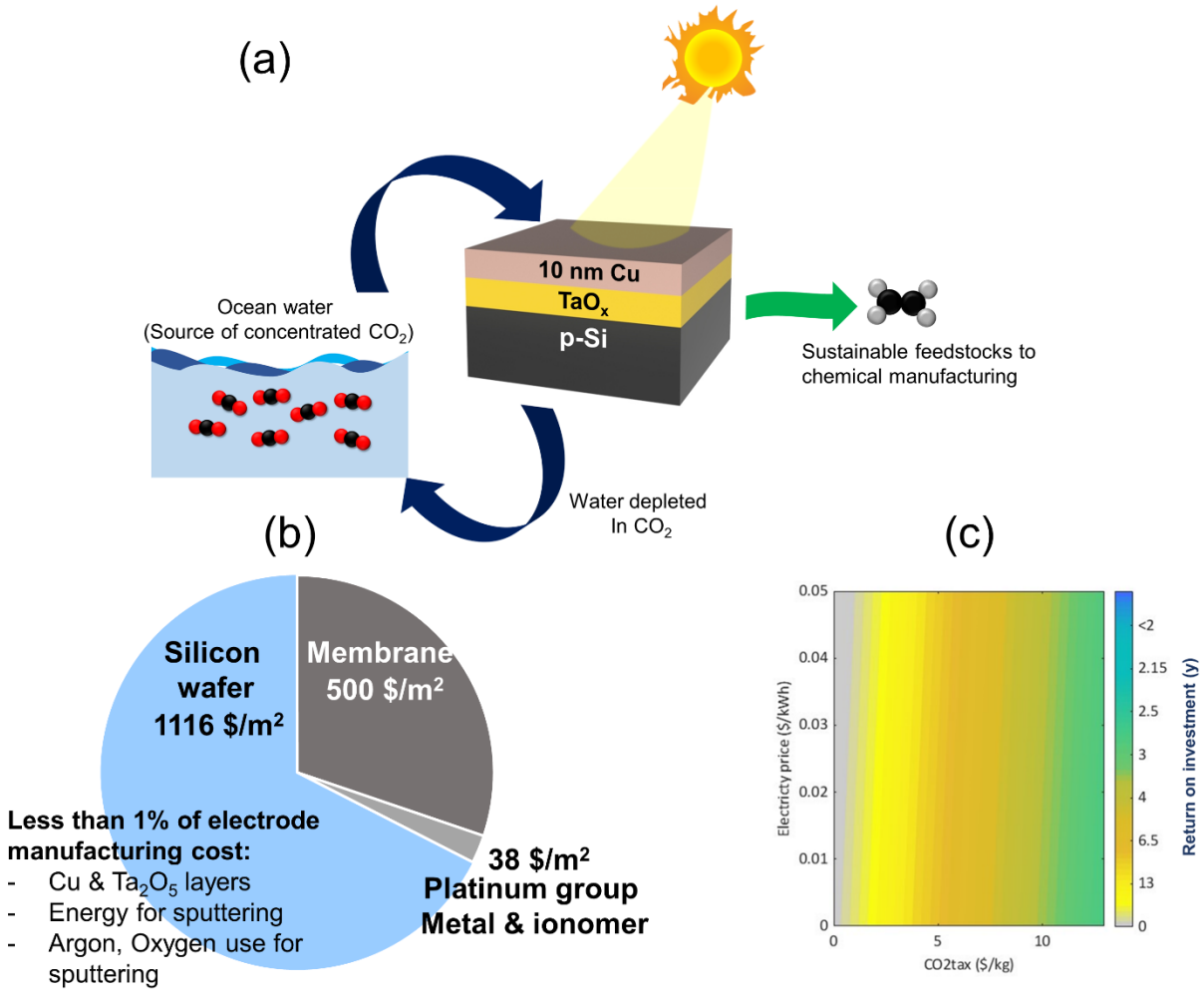


**Figure 9**. Conceptualized scale-up and techno-economic analysis (TEA) of systems incorporating Si/$TaO_x$/Cu photocathodes: (a) concept of biogenic $CO_2$- based manufacturing systems, (b) manufacturing cost for Si/$TaO_x$/Cu photocathodes based on pilot-plant/semi industrial scale coefficient for energy and gases uses during PVD process, (c) sensitivity analysis for the return on investment for the entire photoelectrochemical system, as a function of renewable electricity price and imposed credit for avoided $CO_2$ emissions. Grey area depicts scenarios which are not economically viable. Methodology details are given in the SI.

## CONCLUSIONS

In summary, $TaO_x$ was used as an ETL for Si photocathodes (Si/$TaO_x$ p-n junction) for the first time for $CO_2R$. We first identified the major drawback of employing $TiO_2$ as an ETL (reduction of $TiO_2$ to Ti metal and evolution of $H_2$) and then synthesized $TaO_x$ by 2 different synthesis techniques (PLD and RF sputtering). The electron selectivity of the $TaO_x$ ETLs was tuned by controlling the oxygen partial pressures during thin film deposition for both techniques. Si/$TaO_x$/Cu photocathodes yielded much higher $CO_2R$ products (52% for PLD $TaO_x$ and 30% for RF sputtered $TaO_x$)) when compared with Si/$TiO_2$/Cu photocathode. We also demonstrated a dual ETL layer (Si/$TiO_2$/$TaO_x$/Cu) photocathode which could be a possible strategy for other photocathodes to suppress HER and yield more $CO_2R$ products. The photovoltage of silicon photocathodes with $TaO_x$ ETL/Cu catalyst was improved by using implanted contacts ($n^+$ only on p-Si & $n^+$ and $p^+$ contacts on n-Si) from 300 mV to 430-460 mV. For long term stability of these photocathodes, the limiting factor was the Pt crossover from the counter electrode to the Si/$TaO_x$/Cu photocathode. The photocathode was found to be stable (sustained ethylene production) for ~ 300 mins of $CO_2R$ photoelectrolysis when employing a graphite counter electrode to mitigate Pt crossover. By employing scalable synthesis techniques (RF sputtering for ETLs and Cu catalyst) and simple device architecture without any energy intensive fabrication process (high temperature growth/doping of Si) we have demonstrated an excellent scalability of the system. Our techno-economic analysis outlines pathways to making the photoelectrochemical platform a viable method for decarbonized chemical production, and we determined the scale of $CO_2$ credits mechanisms necessary to support the growth of photocatalytic field. This work also elucidates possible design strategies of other ETLs for $CO_2R$ photocathode- suppression of HER catalysis, good electronic conductivity and Pourbaix stability. Finally, this work raises the question where there are favorable and/or tunable catalyst-metal oxide support interactions in this type of PEC approach and whether

they can be tuned by the choice of metal oxide and by the deposition method. A potential method to investigate such effects would be to use ambient pressure X-ray photoelectron spectroscopy (AP-XPS) to examine the influence of the ETL on the Cu oxidation state under *operando* PEC conditions.

**Author Contributions**

The manuscript was written through contributions of all authors. All authors have given approval to the final version of the manuscript. RL, RRP, and JWA conceived the experiment. RRP, RL and MK performed the synthesis of $TaO_x$. RRP did the XPS measurements and RL performed the UPS measurements. Photocathodes were fabricated by RRP and RL. Liquid and Gas $CO_2R$ product quantification was performed by RRP and RL. SS helped with long-term testing of photocathodes and graphics in the paper. IDT performed the XRD measurements. END performed the MEEP simulations. MB performed the technoeconomic analysis (TEA) and wrote the TEA part. RRP and JWA wrote the original draft of the paper. All authors were involved in the reviewing and editing of the draft. JWA was involved in the funding acquisition and project administration.

**Conflict of interest**

The authors declare no competing financial interests.

**ACKNOWLEDGMENT**

This material is based on work performed by the Liquid Sunlight Alliance, which is supported by the U.S. Department of Energy, Office of Science, Office of Basic Energy Sciences, Fuels from Sunlight Hub under Award Number DE-SC0021266. Technoeconomic analyses performed by MB were supported by the National Research Foundation (NRF), Prime Minister's Office, Singapore, under its Campus for Research Excellence and Technological Enterprise (CREATE) programme through the eCO2EP project NRF2016-ITC001-005 operated by the Cambridge Centre for

Advanced Research and Education in Singapore (CARES) and the Berkeley Educational Alliance for Research in Singapore (BEARS). RRP acknowledges fellowship support from the Swiss National Science Foundation Early Postdoc Mobility Program (191299). MK acknowledges fellowship support from the Brain Korea 21 Program (BK21 FOUR). END acknowledges fellowship support from EPFL and the Heyning-Roelli Schindler Foundation. IDT acknowledges fellowship support from the Erasmus Foundation.

## REFERENCES

1 U. Wurfel, A. Cuevas and P. Wurfel, *IEEE J. Photovoltaics*, 2015, **5**, 461–469.

2 M. Taguchi, A. Yano, S. Tohoda, K. Matsuyama, Y. Nakamura, T. Nishiwaki, K. Fujita and E. Maruyama, *IEEE J. Photovoltaics*, 2014, **4**, 96–99.

3 C. Battaglia, A. Cuevas and S. De Wolf, *Energy Environ. Sci.*, 2016, **9**, 1552–1576.

4 R. V. K. Chavali, S. De Wolf and M. A. Alam, *Prog. Photovoltaics Res. Appl.*, 2018.

5 T. G. Allen, J. Bullock, X. Yang, A. Javey and S. De Wolf, *Nat. Energy*, 2019, **4**, 914–928.

6 G. Campet, C. Puprichitkun and Z. W. Sun, *J. Electroanal. Chem. Interfacial Electrochem.*, 1989, **269**, 435–445.

7 S. Hu, N. S. Lewis, J. W. Ager, J. Yang, J. R. McKone and N. C. Strandwitz, *J. Phys. Chem. C*, 2015, **119**, 24201–24228.

8 S. Chen and L.-W. Wang, *Chem. Mater.*, 2012, **24**, 3659–3666.

9 Y. Lin, C. Battaglia, M. Boccard, M. Hettick, Z. Yu, C. Ballif, J. W. Ager and A. Javey, *Nano Lett.*, 2013, **13**, 5615–5618.

10 Y. Lin, R. Kapadia, J. Yang, M. Zheng, K. Chen, M. Hettick, X. Yin, C. Battaglia, I. D. Sharp, J. W. Ager and A. Javey, *J. Phys. Chem. C*, 2015, **119**, 2308–2313.

11 D. Bae, B. Seger, O. Hansen, P. C. K. Vesborg and I. Chorkendorff, *ChemElectroChem*, 2019, **6**, 106–109.

12 Y. Hori, A. Murata and R. Takahashi, *J. Chem. Soc. Faraday Trans. 1 Phys. Chem. Condens. Phases*, 1989, **85**, 2309.

13 Y. Hori, in *Modern Aspects of Electrochemistry*, Springer New York, New York, NY, 2008, vol. 29, pp. 89–189.

14 Y. Chen, C. W. Li and M. W. Kanan, *J. Am. Chem. Soc.*, 2012, **134**, 19969–19972.

15 N. Han, Y. Wang, H. Yang, J. Deng, J. Wu, Y. Li and Y. Li, *Nat. Commun.*, 2018, **9**, 1320.

16 L. Fan, C. Xia, P. Zhu, Y. Lu and H. Wang, *Nat. Commun.*, 2020, **11**, 3633.

17 S. Nitopi, E. Bertheussen, S. B. Scott, X. Liu, A. K. Engstfeld, S. Horch, B. Seger, I. E. L. L. Stephens, K. Chan, C. Hahn, J. K. Nørskov, T. F. Jaramillo and I. Chorkendorff, *Chem.*

*Rev.*, 2019, **119**, 7610–7672.

18 R. Hinogami, Y. Nakamura, S. Yae and Y. Nakato, *J. Phys. Chem. B*, 1998, **102**, 974–980.

19 J. Qiu, G. Zeng, M.-A. Ha, M. Ge, Y. Lin, M. Hettick, B. Hou, A. N. Alexandrova, A. Javey and S. B. Cronin, *Nano Lett.*, 2015, **15**, 6177–6181.

20 Gurudayal, J. W. Beeman, J. Bullock, H. Wang, J. Eichhorn, C. Towle, A. Javey, F. M. Toma, N. Mathews and J. W. Ager, *Energy Environ. Sci.*, 2019, **12**, 1068–1077.

21 P. B. Pati, R. Wang, E. Boutin, S. Diring, S. Jobic, N. Barreau, F. Odobel and M. Robert, *Nat. Commun.*, 2020, **11**, 3499.

22 Y. Wan, S. K. Karuturi, C. Samundsett, J. Bullock, M. Hettick, D. Yan, J. Peng, P. R. Narangari, S. Mokkapati, H. H. Tan, C. Jagadish, A. Javey and A. Cuevas, *ACS Energy Lett.*, 2018, **3**, 125–131.

23 Y. Wan, J. Bullock and A. Cuevas, *Sol. Energy Mater. Sol. Cells*, 2015, **142**, 42–46.

24 M. T. Greiner, M. G. Helander, W.-M. Tang, Z.-B. Wang, J. Qiu and Z.-H. Lu, *Nat. Mater.*, 2012, **11**, 76–81.

25 T. Wang, S. Liu, H. Li, C. Li, Z. Luo and J. Gong, *Ind. Eng. Chem. Res.*, 2019, **58**, 5510–5515.

26 S. Riyajuddin, J. Sultana, S. A. Siddiqui, S. Kumar, D. Badhwar, S. S. Yadav, S. Goyal, A. Venkatesan, S. Chakraverty and K. Ghosh, *Sustain. Energy Fuels*, 2022, **6**, 197–208.

27 A. Jain, S. P. Ong, G. Hautier, W. Chen, W. D. Richards, S. Dacek, S. Cholia, D. Gunter, D. Skinner, G. Ceder and K. A. Persson, *APL Mater.*, 2013, **1**, 11002.

28 A. K. Singh, L. Zhou, A. Shinde, S. K. Suram, J. H. Montoya, D. Winston, J. M. Gregoire and K. A. Persson, *Chem. Mater.*, 2017, **29**, 10159–10167.

29 J.-Y. Zhang and I. W. Boyd, *Appl. Surf. Sci.*, 2000, **168**, 234–238.

30 X. M. Wu, P. K. Wu, T. -M. Lu and E. J. Rymaszewski, *Appl. Phys. Lett.*, 1993, **62**, 3264–3266.

31 S. J. Song, T. Park, K. J. Yoon, J. H. Yoon, D. E. Kwon, W. Noh, C. Lansalot-Matras, S. Gatineau, H.-K. Lee, S. Gautam, D.-Y. Cho, S. W. Lee and C. S. Hwang, *ACS Appl. Mater. Interfaces*, 2017, **9**, 537–547.

32 Y. R. Denny, T. Firmansyah, S. K. Oh, H. J. Kang, D.-S. Yang, S. Heo, J. Chung and J. C. Lee, *Mater. Res. Bull.*, 2016, **82**, 1–6.

33 R. J. Bondi, M. P. Desjarlais, A. P. Thompson, G. L. Brennecka and M. J. Marinella, *J. Appl. Phys.*, 2013, **114**, 203701.

34 S. Boughaba, M. U. Islam, G. I. Sproule and M. J. Graham, *Surf. Coatings Technol.*, 1999, **120**–**121**, 757–764.

35 E. Atanassova and D. Spassov, *Appl. Surf. Sci.*, 1998, **135**, 71–82.

36 E. Atanassova, T. Dimitrova and J. Koprinarova, *Appl. Surf. Sci.*, 1995, **84**, 193–202.

37 Y. Li, S. Sanna, K. Norrman, D. V. Christensen, C. S. Pedersen, J. M. G. Lastra, M. L. Traulsen, V. Esposito and N. Pryds, *Appl. Surf. Sci.*, 2019, **470**, 1071–1074.

38 A. Paracchino, V. Laporte, K. Sivula, M. Grätzel and E. Thimsen, *Nat Mater*, 2011, **10**, 456–461.

39 M. K. Kovalev, H. Ren, M. Zakir Muhamad, J. W. Ager and A. A. Lapkin, *ACS Energy Lett.*, 2022, **7**, 599–601.

40 O. S. Bushuyev, P. De Luna, C. T. Dinh, L. Tao, G. Saur, J. van de Lagemaat, S. O. Kelley and E. H. Sargent, *Joule*, 2018, **2**, 825–832.

41 Y. Wu, D. C. E. Bakker, E. P. Achterberg, A. N. Silva, D. D. Pickup, X. Li, S. Hartman, D. Stappard, D. Qi and T. Tyrrell, *Commun. Earth Environ. 2022 31*, 2022, **3**, 1–11.

42 M. H. Barecka, J. W. Ager and A. A. Lapkin, *iScience*, 2021, **24**, 102514.

43 K. Kawajiri, K. Tahara and S. Uemiya, *Resour. Environ. Sustain.*, 2022, **7**, 100047.

44 M. Barecka, A. Zieminska and I. Zbicinski, *INREP Proj. Rev. http//www.inrep.eu/files/TCO%202017/INREP_TCO2017_Presentation_TUL_170921.pdf*.

45 Statista, Tantalum price 2021 | Statista, https://www.statista.com/statistics/1009173/tantalum-price/.

46 MacroTrends, Copper Prices - 45 Year Historical Chart | MacroTrends, https://www.macrotrends.net/1476/copper-prices-historical-chart-data.

47 M. Tyson, Silicon Wafer Prices Expected to Increase by up to 25% by 2025 | Tom's Hardware, https://www.tomshardware.com/news/silicon-wafer-prices-expected-to-rise-by-up-to-25-by-2025.

48 A. Mayyas, M. Ruth, B. Pivovar, G. Bender and K. Wipke, Manufacturing Cost Analysis for Proton Exchange Membrane Water Electrolyzers, https://www.nrel.gov/docs/fy10osti/72740.pdf.

49 M. H. Barecka, J. W. Ager and A. A. Lapkin, *STAR Protoc.*, 2021, **2**, 100889.

50 J. G. Vos, T. A. Wezendonk, A. W. Jeremiasse and M. T. M. Koper, *J. Am. Chem. Soc.*, 2018, **140**, 10270–10281.

## GRAPHICAL ABSTRACT